PAPER

Check for updates

Increasing the number of cations in layered double hydroxides *via* mechanochemically complemented synthesis: the more the merrier, or not?†

Evgeniy Seliverstov, [ID] *[a] Maksim Yapryntsev, [ID] [b] Evgeniya Tarasenko [ID] [a] and Olga Lebedeva [ID] [a]

A series of layered double hydroxides Mg/Al, MgNi/Al, MgNi/AlIn, MgNiCo/AlIn, MgNiCo/AlInSc, and MgNiCo/AlInScTm were obtained *via* mechanochemically complemented synthesis with subsequent hydrothermal treatment and additional crystallization. All the samples, except for the Mg/Al one, which was similar to the meixnerite structure, were phase pure. The samples were characterized *via* X-ray diffraction, FTIR spectroscopy, Raman spectroscopy, and transmission electron microscopy. The peroxidase-like activity of the samples was estimated, and the crystal lattice parameters were calculated. Samples with five, six, and seven cations were characterized by X-ray fluorescence, according to which the cation ratios of the samples and the values of configurational entropy were calculated, which allowed them to be classified as high-entropy materials. For the six-cation sample, elemental mapping was additionally performed, which revealed a uniform distribution of elements over the sample area, along with high-temperature X-ray diffraction, which was also carried out for the five-cation sample.

1. Introduction

The term "high-entropy materials" was first applied to high-entropy alloys (HEAs) (also known as multi-major-component alloys) in 2004.[1] Since then, their use and understanding of their properties have expanded significantly. They are multi-component solid solutions that contain five or more elements in near-equiatomic proportions, in which structure stabilization is assumed to occur by maximizing configurational entropy. These new materials are characterized by phase stability and mechanical properties while maintaining high strength and ductility.[2] There are different points of view concerning whether they are stabilized by entropy or not,[3] but at the current moment, the following point of view is predominant. It is proposed to call the new phases formed, because of the configuration entropy, "entropy stabilized" because multicomponent conventional solid solutions also have a high entropy of configuration but are generally not entropy stabilized.[4] However, the name "high-entropy" is still widely used for such materials. Four features are believed to contribute to the excellent performance of HEAs: high entropy, lattice distortion, slow diffusion, and the "cocktail" effect (the synergy of

a mixture of components with the result that is not the mere sum of all components), each of which significantly influences the structural properties of the resulting compound.[5]

In subsequent years, it was possible to obtain high-entropy representatives for other classes of compounds: oxides,[6] metallic glass nanoparticles,[7] borides,[8] sulfides,[9] carbides,[10] nitrides,[11] chalcogenides[12], and antimonides.[13]

Compared with conventional materials, these materials exhibit improved characteristics in various fields of application, such as catalysis,[14] the creation of new electrodes for batteries, supercapacitors, and others.[15] However, only HEAs are well studied, and existing correlations between the structure and characteristics of other classes of high-entropy materials have yet to be explored.

In recent years, there have been reports on other potential substances that could also exist in high-entropy configurations. One of them is the group of layered double hydroxides (LDHs) due to the characteristics of their structure. In addition to high-entropy layered double hydroxides (HE-LDHs), one can find more general term high-entropy hydroxides,[16] including non-layered hydroxides. Layered rare earth hydroxides, as well as their high-entropy representatives, should also be singled out as a separate group.[17]

Layered double hydroxides (LDHs), known as hydrotalcite-like compounds (when produced synthetically), constitute a large family of anionic clay materials. The structure of LDHs includes brucite-like plates separated by anionic particles and water. LDHs with various substituted cations are widely used in many fields, such as catalysis,[18] biomedicine[19] and

[a]Department of General Chemistry, Belgorod State National Research University, Belgorod, 308015, Russia. E-mail: seliverstov.evgeniy.s@gmail.com

[b]Joint Research Centre "Technologies and Materials", Belgorod State National Research University, Belgorod, 308015, Russia

† Electronic supplementary information (ESI) available. See DOI: https://doi.org/10.1039/d4mr00102h

environmental remediation.[20] Additionally, LDHs can be used as precursors for oxide structures such as spinels, where the incorporation of multiple cations into LDHs can be used to tune the final chemical composition of the spinel and its shape and size.[21] HE-LDHs remain insufficiently explored owing to the recent development of this topic and because most studies on LDHs focus on the inclusion of two or three cations, which does not allow them to be classified as high-entropy materials.

The number of cations that must be incorporated to increase entropy varies depending on the structure and sublattice position of the cation.[22] Some authors suggest that for the spinel structure, the difference in high entropy begins with only 7 cations or more.[23] However, other authors have adhered to a more traditional concept in which LDHs with 5 or more cations can be considered high-entropy ones.

To date, several HE-LDHs have been prepared, showing that multication LDHs can act as electrocatalysts and confirming that they can be used as precursors for high-entropy oxides.[24–26]

Typically, layered double hydroxides are synthesized *via* the coprecipitation of metal salts. However, hydroxides of different metals can have quite different pH values of complete precipitation, as well as pH values of dissolution. Considering that high-entropy layered double hydroxides are a multi-metal component system, a high probability of the formation of foreign phases during coprecipitation seems inevitable.

To avoid this, we chose a mechanochemically complemented method of synthesis. According to our assumption, this method allows, owing to the limited volume of water (represented by crystal hydrate water released during the mechanical grinding of salts) in the synthesis space, to increase the probability of the simultaneous incorporation of many different metals into the LDH structure. This method has been successfully applied for the synthesis of non-multicomponent LDHs, with prospects for industrial scaling.[27] Also, the addition of hydrothermal treatment after mechanochemical synthesis is beneficial for the crystallization and regularity of LDHs.[28]

2.   Results and discussion

2.1   X-ray diffraction

According to X-ray diffraction, the reflections of all the samples coincided with those typical for hydrotalcite (Mg/Al LDH, JCPDS card #14-0191) (Fig. 1 (normalized intensity), Fig. S1–S7†). With an increase in the number of cations in the sample, the degree of crystallinity decreases, which is expressed by a decrease and expansion (however, (012), (015) and (018), starting from the five-cation sample, are narrow again) of high-intensity reflections and complete disappearance of low-intensity ones. This can be explained by the fact that distorted by the addition of new elements, the lattice will eventually collapse into an amorphous structure since the lattice distortion energy would be very high for retaining a crystalline configuration. Jien-Wei Yeh also noted the easier formation of amorphous or nano-crystalline (which are not registered by X-rays since they are smaller than their wavelength) structures for a greater number of elements in high-entropy alloys since the growth and even nucleation of crystal phases is gradually inhibited.[29]
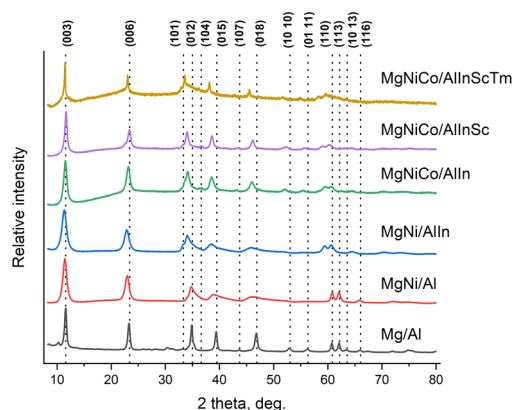

Fig. 1 X-ray diffraction of the LDHs from Mg/Al to MgNiCo/AlInScTm.

A shift of reflections to the left relative to the Mg/Al LDH sample is also noticeable, which is traditionally interpreted in LDHs as an increase in the interlayer space. However, if we zoom in on the most intense reflection (003), on the basis of the position at which the parameter c of the crystal lattice is calculated, the penta- and hexacation samples again shift to the right relative to the others (Fig. 2, normalized). It should be remembered that the cation size is not the only factor influencing the interlayer distance in the LDH structure. A certain influence is exerted by the electrostatic interaction between the brucite-like layers and the interlayer anions, which in turn depends on the uncompensated charge of the layers. Probably, in our samples, a fairly significant distortion of the brucite-like structure is observed, caused by the large number of elements in its composition. In such cases, the correlations among the interlayer distance, the position of reflections, and the number of cations may be absent.

An unexpected result was the production of completely crystalline single-phase samples with 2–7 cations and a trace second phase in the Mg/Al sample. Despite the fact that it was reproduced several times, the presence of a small diffuse phase between 25 and 35° (2 theta) was detected. This sample itself is remarkable in that, according to the Match databases, it completely corresponds to meixnerite (JCPDS card #38-0478),
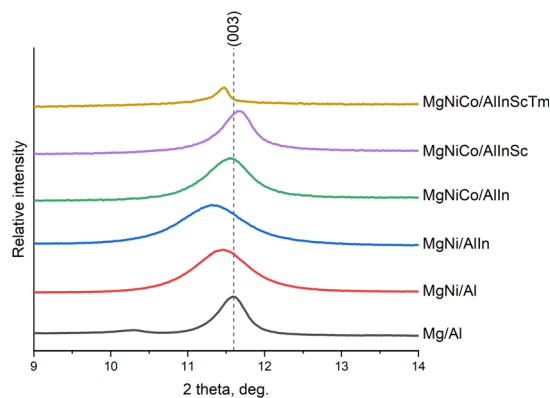

Fig. 2 Close-up of the (003) reflection of synthesized LDHs.

a natural LDH with the formula $Mg_6Al_2(OH)_{18}\cdot4H_2O$. Meixnerite is very difficult to obtain synthetically since this type of compound has only OH^- as a compensating anion, which can usually be achieved only in a carbonate-free environment.

However, there are articles describing such synthesis, and the article by Pavel *et al.* shows a diffraction pattern of synthetic meixnerite, which also has a foreign phase similar to that found in our sample, which the authors attributed to the broad and very low intensity diffraction of amorphous $Al(OH)_3$.[30] Tongamp *et al.* succeeded in obtaining meixnerite by the mechanochemical method.[31]

Notably, our Mg/Al LDH sample, as well as the typical meixnerite diffraction pattern from the JCPDS database, contains rare characteristic LDH reflections such as (101), (107), (10.10), (10.13), and (116). The reflection (104) is recorded only for the MgNiCo/AlIn and MgNiCo/AlInSc samples. The peak at approximately 11° (2 theta) may indicate the presence of two anions in the interlayer space of Mg/Al sample. In the case of our sample, we assume that the second anion is the residual amount of nitrate anions from the original salts used in the synthesis.

2.2 Crystal lattice parameters

For the heptacation sample (MgNiCo/AlInScTm), it was possible to calculate only the degree of crystallinity and the lattice parameter c because of the low intensity and broadening of the XRD reflections (Table 1). The (110) reflection, necessary for calculating the lattice parameter a, which characterizes the distance between neighboring cations, was represented by a wide rise in the XRD data line, probably combining broadened reflections (110), (113), and (10.13). This is explained by the random arrangement of thulium cations with very different ionic radii in the crystal lattice, which causes different X-ray diffractions in different places of the sample crystals, leading to broadening of the reflections.

The average crystallite size agreed well with the data calculated *via* the Scherrer equation and the Halder–Wagner–Landford (HWL) method. First, a decrease in the crystallite size is observed from the two-cation (Mg/Al LDH) to the four-cation (MgNi/AlIn LDH) samples. The opposite trend is then observed, where starting from the five-cation (MgNiCo/AlIn) sample, there is an increase in the average crystallite size. It was expected that the microstrain value would increase with the number of cations, but its highest value was observed for the

four-cation sample, after which it began to decrease without reaching, however, the value calculated for the two- and three-cation samples.

The degree of crystallinity was expectedly high for the two-, three-, and four-cation samples, after which it began to decrease.

The parameter a of the crystal lattice increased throughout the entire series of LDH samples, which indicates an increase in the distance between neighboring cations in the crystal lattice with increasing number of cations with different ionic radii.

The parameter c, which characterizes the interplanar distance of the brucite-like LDH layers, tended to increase in the three-cation sample and further decreased up to the seven-cation sample, where its increase was again observed.

The volume V of the unit cell was the largest in the four-cation sample, after which it began to decrease.

It should be noted that the cell parameters of Mg/Al LDH were closer to those of meixnerite than to those of hydrotalcite, which serves as additional confirmation of its formation in the course of our work.[32]

2.3 FTIR spectroscopy

All the samples show a typical pattern for the FTIR spectra of the layered double hydroxides (Fig. 3, normalized). The broad absorption band at approximately 3500 cm^{-1} is attributed to O–H stretching vibrations. Overlapping of the stretching vibrations of structural OH^- and physically adsorbed water and the vibrations of OH^- bonded with carbonate ions caused broadening. A weak band at approximately 3000 cm^{-1} can be related to solvation water molecules in the micropores of the
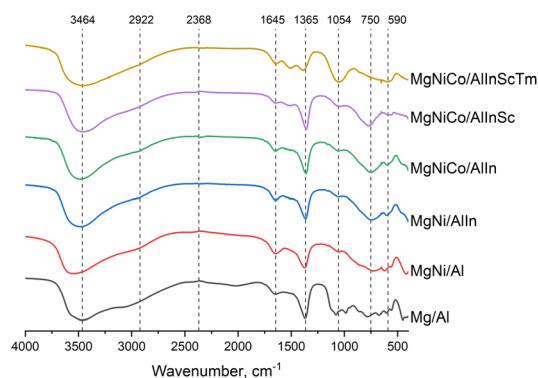

Fig. 3 FTIR spectroscopy of LDHs from Mg/Al to MgNiCo/AlInScTm.

Table 1 Crystal lattice parameters of the samples^a

Sample	Average crystallite size, nm	Microstrain, $\times 10^{-3}$	Crystallinity index%	a, Å	c, Å	V, Å^3
Mg/Al	17.3 (19.6*)	5.1	77.6	3.04	22.63	181.7
MgNi/Al	8.4 (9.4*)	3.3	83.4	3.05	23.35	188.4
MgNi/AlIn	7.4 (8.4*)	14.3	78.5	3.11	23.31	195.2
MgNiCo/AlIn	9.8 (11.4*)	13.1	66.9	3.12	23.06	194.1
MgNiCo/AlInSc	12.9 (14.5*)	9.9	63.9	3.13	22.75	192.7
MgNiCo/AlInScTm	—	—	53.2	—	23.06	—

^{a} *Calculated with the HWL method.

LDH structure.[33] In our experience, weak peaks at approximately 2400 cm^{-1} are possibly related to CO_2 molecules physically adsorbed from the air. The bending vibration of the water interlayer was reflected at 1645 cm^{-1}. The absorption band at approximately 1365 cm^{-1} is related to carbonate anions. The following bands at a lower wavenumber are typically attributed to Me–O and O–Me–O stretching vibrations.[34] The band broadening at approximately 1054 cm^{-1} for MgNiCo/AlInScTm is possibly caused by the incorporation of large Tm cations into the octahedral layers.

2.4 Raman spectroscopy

Fig. 4 shows the normalized Raman spectra of the obtained LDHs. The band at approximately 483 cm^{-1} can be attributed to vibrations of the Me–O–Me present in the brucite-like layers of the LDHs. In the region of approximately 518 cm^{-1}, a characteristic band of the octahedral structure of the brucite-like layers is observed, *i.e.*, stretching of Me^{2+}–O–Me^{3+} bonds.[35] The band in the region of 1050 cm^{-1} is characteristic of all intercalated anions; in the case of our samples, it is represented by carbonate anions. The signal at the lower wavenumber (approximately 950 cm^{-1}) can be assigned to carbonate ions that are bonded to neither brucite-like layers nor interlayer water, whereas that at the higher wavenumber corresponds to carbonate ions that are strongly hydrogen-bonded to water molecules.[36] Notably, a single signal was present in the Mg/Al sample at about 950 cm^{-1}, whereas the other signals were absent. Since meixnerite does not have carbonate anions in the interlayer space, the absence of a signal in the region of 1050 cm^{-1} is expected, but at the moment we find it difficult to explain the nature of the absence of other peaks characteristic of brucite-like LDH layers, since we have not found examples of recorded Raman spectra for minerals of the meixnerite type for comparison.

The signal intensity of the remaining samples does not correlate with the increase in the number of cations and most likely depends only on the nature of the introduced cations.

2.5 Transmission electron microscopy

Morphologically, the obtained samples are represented by particles with shapes close to hexagonal, which is typical for
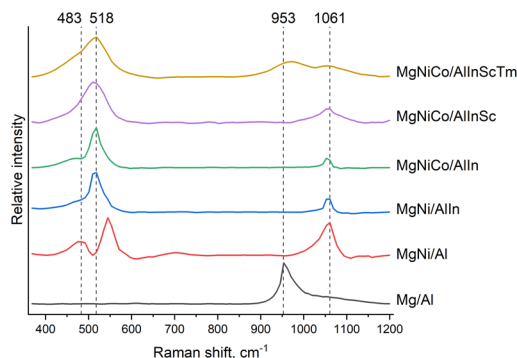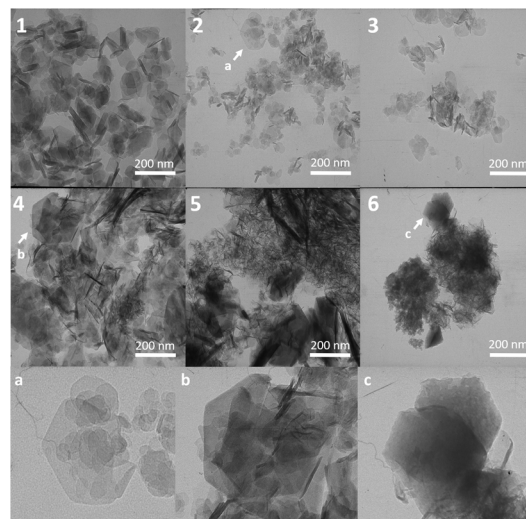

Fig. 5 Transmission electron microscopy pictures: 1 – Mg/Al, 2 – MgNi/Al, 3 – MgNi/AlIn, 4 – MgNiCo/AlIn, 5 – MgNiCo/AlInSc, 6 – MgNiCo/AlInScTm; (a) – close-up of part of picture 2, (b) – close-up of part of picture 4, (c) – close-up of part of picture 3.

LDHs (Fig. 5 1–6). The most clearly expressed plates are observed in two-, three- and four-cation samples; in the subsequent samples, very small particles of nanometer size and large layered agglomerates can be observed. However, individual large hexagonal particles with a diameter of 150–200 nm fall into the field of view (Fig. 5a–c), the presence of which is recorded even in the seven-cation sample MgNiCo/AlInScTm.

2.6 Elemental mapping

Elemental mapping of the hexacation MgNiCo/AlInSc LDH sample revealed the presence of all the elements incorporated during the synthesis and revealed the homogeneous distribution of all six cations in the sample (Fig. 6).

2.7 Me^{2+}/Me^{3+} ratio and configurational entropy

The S_{conf} and Me^{2+}/Me^{3+} ratio values were calculated for the penta-, hexa-, and heptacation samples according to the X-ray fluorescence data (Table 2). For the hexacation sample, EDAX was also performed. The obtained ratios of divalent cations to
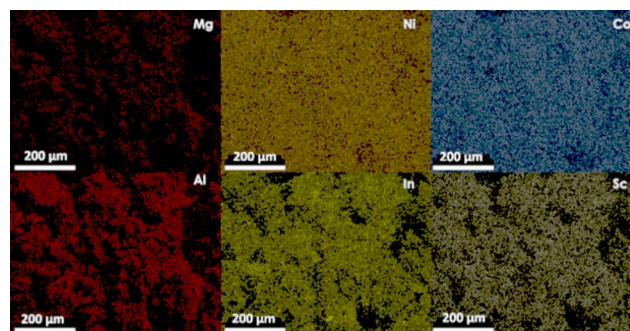

Fig. 4 Raman spectroscopy of LDHs from Mg/Al to MgNiCo/AlInScTm.

Fig. 6 Elemental distribution of the MgNiCo/AlInSc.

Table 2 Calculated entropy and the cation ratio of the samples

LDH sample	S_{conf}	Expected Me^{2+}/Me^{3+} ratio	Experimental Me^{2+}/Me^{3+} ratio
MgNiCo/AlIn	1.52 R	3:1	3.7:1
MgNiCo/AlInSc	1.56 R (1.62 R[a])	3:1	3.2:1 (2.9:1[a])
MgNiCo/AlInScTm	1.62 R	3:1	3.5:1
Mg/Al	0.57 R[b]	3:1	—
MgNi/Al	1.08 R[b]	3:1	—

[a] According to EDAX data. [b] Evaluative calculation.

trivalent cations for all three LDHs lie in the range of 3–3.7:1, corresponding to 1.5–4:1, which is acceptable for the formation of LDHs.[37]

The S_{conf} for all three samples exceeds 1.5 R, which allows them to be classified as high-entropy materials according to the classification of entropy degrees by Murty *et al.*[38] Notably, the sample with five cations, MgNiCo/AlIn, is essentially on the border between high and medium entropy values. The actual molar fractions of elements in the resulting synthetic LDHs are often lower than those initially assumed during their synthesis, so we admit the possibility of obtaining a five-cation sample, which will nevertheless have the S_{conf} of the medium-entropy material. Remembering that the value of the configurational entropy is affected by both the equimolar ratio of elements and their number, and taking into account the classification of Zhang *et al.*, it can be assumed that it is more reliable to consider LDHs with a cation number $\geq$ 6 as high-entropy, but for them, it is also necessary to measure the actual molar fractions of elements in the composition.[39]

2.8 Cation mole fractions

Based on the X-ray fluorescence analysis of the MgNiCo/AlIn, MgNiCo/AlInSc, and MgNiCo/AlInScTm LDH samples, which showed a configurational entropy value that allows them to be classified as high-entropy materials, mole fractions were calculated separately for divalent and trivalent cations (Table 3). Overall, the results were close to the precalculated equimolar values with a few exceptions. The magnesium in the six-cation sample and scandium in the seven-cation sample turned out to be significantly less than the precalculated values, while the percentage of thulium in the total amount of trivalent cations of the seven-cation sample turned out to be higher than it was expected.

This confirms our opinion that when synthesizing high-entropy LDHs, one should focus on both the equimolar ratio of cations and their number, since due to the uneven incorporation of cations into the crystal lattice of LDHs, there is a possibility of obtaining a pentacation but not high-entropy sample if several of the cations are incorporated in small quantities.

2.9 High-temperature X-ray diffraction

A study of the thermal transformations of MgNiCo/AlInSc (Fig. 7) and MgNiCo/AlIn LDHs (Fig. 8) revealed that the samples behave in a typical manner for LDHs when heated — at temperatures above 200 °C, they decompose through the stage of metastable dehydrated forms with the final formation of nonstoichiometric mixed oxides during subsequent heating. In case of high-entropy LDHs these oxides are also correspondent high-entropy oxides.[26]

2.10 Peroxidase-like activity

Tetramethylbenzidine (TMB) acts as an electron donor for the reduction of hydrogen peroxide to water by the five-, six-, and seven-cation LDHs. The resulting one-electron oxidation
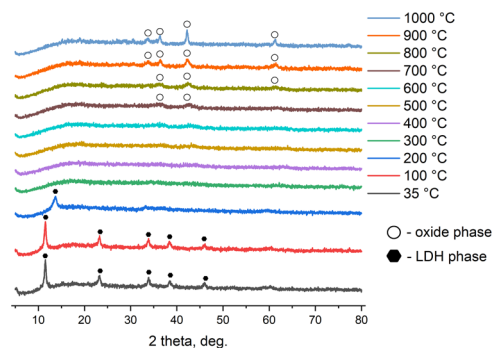

Fig. 7 High-temperature X-ray diffraction of MgNiCo/AlInSc.

Table 3 Composition of high-entropy LDHs

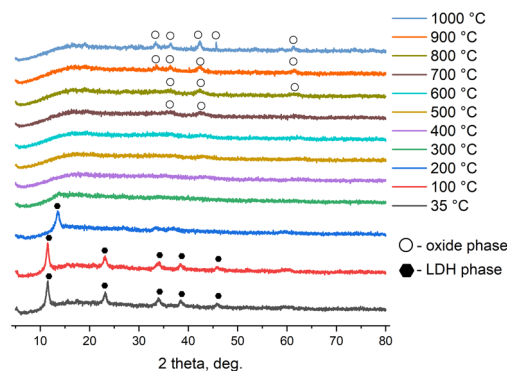|	Mole fractions, experimental (expected), %						
	Divalent cations				Trivalent cations		
Sample	Mg	Ni	Co	Al	In	Sc	Tm
MgNiCo/AlIn	27.8 (33.4)	36.7 (33.3)	35.4 (33.3)	50 (50)	50 (50)	—	—
MgNiCo/AlInSc	13.2 (33.4)	46 (33.3)	40.8 (33.3)	37.5 (33.4)	37.5 (33.3)	25 (33.3)	—
MgNiCo/AlInScTm	28.2 (33.4)	37.2 (33.3)	34.6 (33.3)	40.9 (31.7)	45.4 (31.7)	4.5 (31.7)	9.1 (5)

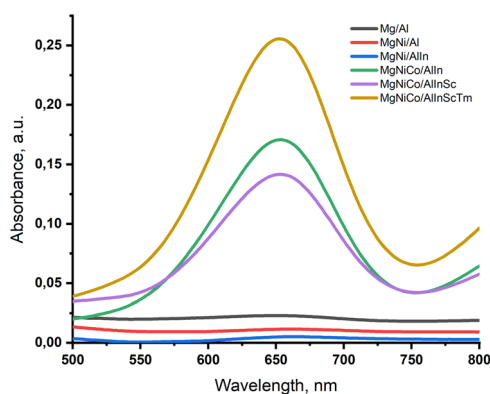Fig. 8 High-temperature X-ray diffraction of MgNiCo/AlIn.

Fig. 9 Spectrum of the TMB solution after the addition of LDHs.

Fig. 10 Pictures of LDHs powders, from left to right: Mg/Al, Mg/Ni/Al, MgNi/AlIn, MgNiCo/AlIn, MgNiCo/AlInSc, and MgNiCo/AlInScTm.

mechanochemical synthesis with subsequent soft hydrothermal treatment and additional crystallization in a saturated alkali solution. The expanded description of the synthesis has been added to the ESI.†

During the synthesis, we adhered to the classic molar ratio of elements for LDHs of $3:1$ for $Me^{2+}:Me^{3+}$, respectively. All divalent elements, as well as trivalent ones, were taken in equimolar ratios to each other. Thulium was an exception because, in our previous studies, we showed that it is possible to achieve a single-phase sample of LDHs with no more than 5% of rare-earth metal cations included in the crystal lattice, with few exceptions.[40] However, according to our experience, for scandium, it is possible to achieve even binary Mg/Sc LDH.[41] In turn, for indium we also obtained well-crystallized samples of Co/In LDH.[42] Reagents were mixed in an agate mortar and manually ground for 5 minutes at room temperature. After a homogeneous powder was obtained, Na_2CO_3 (25 mmol) and NaOH (5 mmol) were added to it, which was subsequently ground for 30 minutes to obtain a viscous homogeneous paste. The paste was washed with distilled water (100 ml) into the hydrothermal synthesis vessel. The vessel was sealed and left for one day at 98 °C. We found experimentally that adding a saturated alkaline solution in the middle of the hydrothermal treatment promoted the crystallization of the samples (Fig. S0†). We hypothesized that this was due to hydroxyl adsorption, which increases with increasing pH which was lowered by the previous water dilution step. So, after 24 hours, the vessel was opened, and a 0.1 M Na_2CO_3 (100 ml) solution was added to the reaction mixture, which was left for two days at 98 °C. The mixture was then kept in a cooling vessel for another day, after which the resulting precipitate was separated by centrifugation, washed with distilled water until a neutral pH was reached, and then dried at 50 °C.

product is a diimine–diamine complex with a blue color, resulting in the appearance of a characteristic absorption maximum at a wavelength of 650 nm (Fig. 9).

Presumably, this occurs due to the incorporation of the cobalt cation Co^{2+}, which is able to reduce hydrogen peroxide. In this case, one could expect a decrease in the degree of oxidation of the dye with an increase in the number of cations.

However, Fig. 9 shows that the intensity of the maximum of the colored fraction of the dye in the solution decreases slightly from the five- to six-cation samples and increases with the incorporation of thulium cations into the LDH.

3. Materials and methods

3.1 Synthesis

The following reagents were used: magnesium(II) nitrate hexahydrate $Mg(NO_3)_2 \cdot 6H_2O$, nickel(II) nitrate hexahydrate $Ni(NO_3)_2 \cdot 6H_2O$, cobalt(II) nitrate hexahydrate $Co(NO_3)_2 \cdot 6H_2O$, aluminum(III) nitrate nonahydrate $Al(NO_3)_3 \cdot 9H_2O$, indium(III) nitrate 4,5-hydrate $In(NO_3)_3 \cdot 4.5H_2O$, scandium(III) nitrate tetrahydrate $Sc(NO_3)_3 \cdot 4H_2O$, thulium(III) nitrate pentahydrate $Tm(NO_3)_3 \cdot 5H_2O$, sodium hydroxide NaOH, and sodium carbonate Na_2CO_3.

All the samples (Fig. 10), from left to right: Mg/Al, MgNi/Al, MgNi/AlIn, MgNiCo/AlIn, MgNiCo/AlInSc, MgNiCo/AlInScTm were synthesized *via* a method generally described as manual

3.2 Data processing and visualization

The data were graphed and analysed *via* OriginPro software (Version 2021, OriginLab Corporation, Northampton, MA, USA).

3.3 Configurational entropy calculation

Currently, work on mathematical models for calculating the entropy of crystalline substances is still in progress. Various calculation methods yield a wide range of results depending on the chosen technique. Thus, the considered technique may not

be universal and provides only selective consistency with the experiment.

The most common method is the calculation of configurational entropy S_{conf}.[39] In the case of high-entropy alloys, the term entropy of mixing S_{mix} also exists.[38] It can take into account the anions included:

$$S_{conf} = -R\left[\left(\sum_{i=1}^{N} x_i \ln x_i\right)_{\text{cation-site}} + \left(\sum_{j=1}^{N} x_j \ln x_j\right)_{\text{anion-site}}\right]$$

Here, R is the universal gas constant, and x_i and x_j are the mole fractions of elements in the cationic and anionic units, respectively. This formula has been proposed for use with high-entropy oxides.[43,44] It is also proposed to consider the number of possible configurations of structural elements in all sublattices of the compound when calculating the configurational entropy of complex compounds.[22]

However, we assume that in the case of layered double hydroxides, otherwise called anion-exchange clays, the contribution of anions to the total entropy of the system can vary significantly, since their position between layers is unstable, and both their nature and quantity can change even within the same sample during its use and storage.

Thus, in our work, we calculate only the configurational entropy of cations in the brucite-like layers of LDH:

$$S_{conf} = -R\sum_{i=1}^{N} x_i \ln x_i$$

It is proposed what alloys with $S_{conf} < 1$ R are low-entropy, those with 1 R $\leq S_{conf} \leq 1.5$ R are medium-entropy, and those with $S_{conf} \geq 1.5$ R are high-entropy.[38] This decrease in free energy causes the solid solution phases to have a greater ability to compete with intermetallic compounds. This means that the tendency to form the mixing state of elements increases with increasing S_{conf}.

However, this entropy borderline has not yet been established, and one can find also a definition of it as $S_{conf} \geq 1.61$ R for high-entropy materials.[39]

The configurational entropy calculation example has been added to the ESI.†

3.4 X-ray fluorescence

X-ray fluorescence analysis of the MgNiCo/AlIn, MgNiCo/AlInSc, and MgNiCo/AlInScTm LDH's samples was performed on an ARL™ PERFORM'X Sequential X-Ray Fluorescence Spectrometer (Thermo Fisher Scientific, 2012).

3.5 X-ray crystallography

X-ray diffraction (XRD) analysis was carried out via a Rigaku Ultima IV X-ray diffractometer with CuKα ($\lambda = 015\,418\,740$ nm) radiation (Rigaku, 2008). The patterns were scanned from 5 to 80° (2θ) at a step size of 0.02° (2θ).

The phase analysis was performed in Match! software with PDF-2 diffraction database using powder diffraction data.[45]

The XRD profiles were compared to standards compiled by the Joint Committee on Powder Diffraction and Standards (JCPDS), which included cards #14-0191 for hydrotalcite and #38-0478 for meixnerite.

The average crystallite size was calculated via the Scherrer equation and Halder–Wagner–Landford method, which was also used to calculate the microstrain. A link to the method has been added to the ESI.†

The basal (003) reflection corresponds to successive orders of the basal spacing $c = 3d_{(003)}$. The intense (110) reflection utilized for the calculation of the lattice parameter $a = 2d_{(110)}$ depends on the ionic radius of the cations included.[46]

The crystallinity index was calculated as the ratio of the crystalline XRD peak area to the crystalline plus amorphous peaks of the obtained XRD data. A link to the method has been added to the ESI.†

The unit cell volume (V) was also calculated via the following equation:[47]

$$V = a^2 c \sin 60°$$

3.6 High-temperature X-ray diffraction

All the equipment and parameters were the same as those used for the XRD analysis. The patterns were scanned first at 35 °C, and then in the range of 100–1000 °C at a step size of 100 °C. The heating rate was 25 °C per minute, and the holding time at each temperature was 10 minutes.

3.7 Transmission electron microscopy

The morphology of the obtained LDHs was studied via a JEM-2100 electron microscope (JEOL, Japan, 2007). One drop of a sample suspension in anhydrous isopropyl alcohol, pretreated in an ultrasonic bath, was applied to a copper mesh coated with a thin carbon film. A few images at 50k× and 100k× magnification were taken from each sample. Additionally, energy dispersive X-ray (EDX) analysis with element mapping of 12 different points on a sample was performed to characterize the elemental composition of the 6-cation sample MgNiCo/AlInSc.

3.8 FTIR spectroscopy

IR spectra of the synthesized LDHs were obtained on an FSM 2201 Fourier spectrometer (INFRASPEK, Russia). The samples were prepared by pressing a mixture of potassium bromide with the synthesized sample at a ratio of 300 : 1.

3.9 Raman spectroscopy

Raman spectra were recorded on a LabRam HR Evolution Raman confocal microspectrometer (HORIBA Jobin Yvon S.A.S., Japan). The patterns were scanned via a green Nd:YAG laser with a wavelength of 532 nm in the range of 200–2000 cm^{-1}.

3.10 Peroxidase-like activity evaluation

The peroxidase-like activity of the obtained samples was assessed via a ready-made stabilized aqueous solution of 3,3′,5,5′-tetramethylbenzidine (TMB) (TMB Core+, Bio-Rad, USA). The typical process was implemented as follows: 2 ml of

TMB solution and 0.002 grams of sample were mixed and incubated for 30 minutes at 35 °C. The characteristic absorbance of oxidized TMB at approximately 650 nm was measured *via* a UV-Vis spectrophotometer (Specord 210 plus) (Analytik Jena, Germany, 2014).

4. Conclusions

In our study, we demonstrated the possibility of obtaining phase-pure layered double hydroxides with several cations ranging from two to seven *via* a mechanochemically complemented synthesis with subsequent hydrothermal treatment and additional crystallization. Due to the greater affinity of LDHs for carbonate anions than for nitrate ones, and the large amount of sodium carbonate used in the synthesis of our samples, we assume that the majority of anions in our samples are carbonate with some nitrate anion residues.

With an increase in the number of cations, a decrease in the degree of crystallinity of the samples was noted.

According to X-ray diffraction and calculations of the crystal lattice parameters, the two-cation sample was more similar to meixnerite than to hydrotalcite. Thus, we additionally demonstrated the possibility of synthesizing a meixnerite-like material *via* the described method.

The calculated S_{conf} values allow us to classify samples with ≥ 5 cations as high-entropy materials; however, this threshold is taken from the field of alloy research, and mathematical models of entropy changes have not yet been developed for crystalline substances. Some trends in the changes in sample characteristics and properties, such as the average crystallite size, microstrain, lattice parameter c, cell unit volume, and peroxidase-like activity, broke when the number of cations was increased to four or five.

However, this may depend on the properties of the included cation rather than on the synergistic properties of the high-entropy system.

Data availability

Data for this article, including X-ray diffraction, FTIR and Raman spectroscopy, TEM pictures and elemental mapping are available at Mendeley Data at **https://doi.org/10.17632/rbkchr9byr.1**.

Author contributions

Evgeniy Seliverstov — conceptualization, investigation, methodology, visualization, writing — original draft; Maksim Yapryntsev — formal analysis, resources; Evgeniya Tarasenko — formal analysis, resources; Olga Lebedeva — project administration, resources, supervision, writing — review & editing.

Conflicts of interest

There are no conflicts to declare.

Acknowledgements

References

1 B. Cantor, I. T. H. Chang, P. Knight and A. J. B. Vincent, Microstructural development in equiatomic multicomponent alloys, *J. Mater. Sci. Eng. A*, 2004, **375–377**, 213–218.

2 Z. Li, K. G. Pradeep, Y. Deng, D. Raabe and C. C. Tasan, Metastable high-entropy dual-phase alloys overcome the strength–ductility trade-off, *Nature*, 2016, **534**, 227–230.

3 T. Löffler, A. Savan, A. Garzón-Manjón, M. Meischein, C. Scheu, A. Ludwig and W. Schuhmann, Toward a paradigm shift in electrocatalysis using complex solid solution nanoparticles, *ACS Energy Lett.*, 2019, **4**, 1206–1214.

4 N. Dragoe and D. Bérardan, Order emerging from disorder, *Science*, 2019, **366**, 573–574.

5 D. B. Miracle and O. N. Senkov, A critical review of high entropy alloys and related concepts, *Acta Mater.*, 2017, **122**, 448–511.

6 C. M. Rost, E. Sachet, T. Borman, A. Moballegh, E. C. Dickey, D. Hou, J. L. Jones, S. Curtarolo and J.-P. Maria, Entropy-stabilized oxides, *Nat. Commun.*, 2015, **6**, 8485.

7 M. W. Glasscott, A. D. Pendergast, S. Goines, A. R. Bishop, A. T. Hoang, C. Renault and J. E. Dick, Electrosynthesis of high-entropy metallic glass nanoparticles for designer, multi-functional electrocatalysis, *Nat. Commun.*, 2019, **10**, 2650.

8 J. Gild, Y. Zhang, T. Harrington, S. Jiang, T. Hu, M. C. Quinn, W. M. Mellor, N. Zhou, K. Vecchio and J. Luo, High-entropy metal diborides: a new class of high-entropy materials and a new type of ultrahigh temperature ceramics, *Sci. Rep.*, 2016, **6**, 2–11.

9 R.-Z. Zhang, F. Gucci, H. Zhu, K. Chen and M. J. Reece, Data-driven design of ecofriendly thermoelectric high-entropy sulfides, *Inorg. Chem.*, 2018, **57**, 13027–13033.

10 P. Sarker, T. Harrington, C. Toher, C. Oses, M. Samiee, J.-P. Maria, D. W. Brenner, K. S. Vecchio and S. Curtarolo, High-entropy high-hardness metal carbides discovered by entropy descriptors, *Nat. Commun.*, 2018, **9**, 4980.

11 T. Jin, X. Sang, R. R. Unocic, R. T. Kinch, X. Liu, J. Hu, H. Liu and S. Dai, Mechanochemical-assisted synthesis of high-entropy metal nitride *via* a soft urea strategy, *Adv. Mater.*, 2018, **30**, 1707512.

12 M. A. Buckingham, B. Ward-O'Brien, W. Xiao, Y. Li, J. Qu and D. J. Lewis, High entropy metal chalcogenides: synthesis, properties, applications and future directions, *Chem. Commun.*, 2022, **58**, 8025–8037.

13 L. Ren, J. Liu, X. Liu, J. Luo and J. Li, Rapid synthesis of high-entropy antimonides under air atmosphere using microwave method to ultra-high energy density supercapacitors, *J. Alloys Compd.*, 2023, **967**, 171816.

14 Y. Sun and S. Dai, High-entropy materials for catalysis: a new frontier, *Sci. Adv.*, 2021, **7**, eabg1600.

15 M. Fu, X. Ma, K. Zhao, X. Li and D. Su, High-entropy materials for energy-related applications, *Iscience*, 2021, **24**, 102177.

16 A. J. Knorpp, P. Allegri, S. Huangfu, A. Vogel and M. Stuer, Synthesis and Characterization of High-Entropy Dawsonite-Type Structures, *Inorg. Chem.*, 2023, **62**, 4999–5007.

17 M. A. Teplonogova, A. D. Yapryntsev, A. E. Baranchikov and V. K. Ivanov, High-entropy layered rare earth hydroxides, *Inorg. Chem.*, 2022, **61**, 19817–19827.

18 G. Fan, F. Li, D. G. Evans and X. Duan, Catalytic applications of layered double hydroxides: recent advances and perspectives, *Chem. Soc. Rev.*, 2014, **43**, 7040–7066.

19 G. Arrabito, A. Bonasera, G. Prestopino, A. Orsini, A. Mattoccia, E. Martinelli, B. Pignataro and P. G. Medaglia, Layered double hydroxides: a toolbox for chemistry and biology, *Crystals*, 2019, **9**, 361.

20 A. M. Cardinale, C. Carbone, S. Consani, M. Fortunato and N. Parodi, Layered double hydroxides for remediation of industrial wastewater from a Galvanic plant, *Crystals*, 2020, **10**, 443.

21 F. Li, J. Liu, D. G. Evans and X. Duan, Stoichiometric Synthesis of Pure MFe2O4 (M = Mg, Co, and Ni) Spinel Ferrites from Tailored Layered Double Hydroxide (Hydrotalcite-Like) Precursors, *Chem. Mater.*, 2004, **16**, 1597–1602.

22 O. F. Dippo and K. S. Vecchio, A universal configurational entropy metric for high-entropy materials, *Scr. Mater.*, 2021, **201**, 113974.

23 A. J. Knorpp, A. Zawisza, S. Huangfu, A. Borzì, A. H. Clark, D. Kata, T. Graule and M. Stuer, Hydrothermal synthesis of multi-cationic high-entropy layered double hydroxides, *RSC Adv.*, 2022, **12**, 26362–26371.

24 A. Miura, S. Ishiyama, D. Kubo, N. C. Rosero-Navarro and K. Tadanaga, Synthesis and ionic conductivity of a high-entropy layered hydroxide, *J. Ceram. Soc. Jpn.*, 2020, **128**, 336–339.

25 K. Gu, X. Zhu, D. Wang, N. Zhang, G. Huang, W. Li, P. Long, J. Tian, Y. Zou, Y. Wang, R. Chen and S. Wangl, Ultrathin defective high-entropy layered double hydroxides for electrochemical water oxidation, *J. Energy Chem.*, 2021, **60**, 121–126.

26 M. Kim, I. Oh, H. Choi, W. Jang, J. Song, C. S. Kim, J.-W. Yoo and S. Cho, A solution-based route to compositionally complex metal oxide structures using high-entropy layered double hydroxides, *Cell Rep. Phys. Sci.*, 2022, **3**, 100702.

27 O. B. Belskaya and V. A. Likholobov, Mechanochemical synthesis of layered double hydroxides as a promising method for the preparation of adsorbents and catalysts, *Kinet. Catal.*, 2022, **63**, 615–641.

28 X. Zhang and S. Li, Mechanochemical approach for synthesis of layered double hydroxides, *Appl. Surf. Sci.*, 2013, **274**, 158–163.

29 Y. E. H. Jien-Wei, Recent progress in high entropy alloys, *Ann. Chim.: Sci. Mater.*, 2006, **31**, 633–648.

30 O. D. Pavel, R. Zăvoianu, R. Bîrjega, E. Angelescu, G. Costentin and M. Che, Exploring an alternative route for meixnerite synthesis. The impact of the gaseous environment on the reconstruction of the lamellar structure and the catalytic performances, *Appl. Clay Sci.*, 2015, **104**, 59–65.

31 W. Tongamp, Q. Zhang and F. Saito, Preparation of meixnerite (Mg–Al–OH) type layered double hydroxide by a mechanochemical route, *J. Mater. Sci.*, 2007, **42**, 9210–9215.

32 S. J. Mills, A. G. Christy, J. M. Génin, T. Kameda and F. Colombo, Nomenclature of the hydrotalcite supergroup: natural layered double hydroxides, *Mineral. Mag.*, 2012, **76**, 1289–1336.

33 L. Châtelet, J. Y. Bottero, J. Yvon and A. Bouchelaghem, Competition between monovalent and divalent anions for calcined and uncalcined hydrotalcite: anion exchange and adsorption sites, *Colloids Surf., A*, 1996, **111**, 167–175.

34 M. Shabanian, M. Hajibeygi and A. Raeisi, FTIR characterization of layered double hydroxides and modified layered double hydroxides, *Layered Double Hydroxide Polymer Nanocomposites*. Woodhead Publishing, 2020, pp. 77–101.

35 L. P. F. Benício, D. Eulálio, L. de M. Guimarães, F. G. Pinto, L. M. da Costa and J. Tronto, Layered double hydroxides as hosting matrices for storage and slow release of phosphate analyzed by stirred-flow method, *Mater. Res.*, 2018, **21**, e20171004.

36 S. J. Palmer, R. L. Frost and H. J. Spratt, Synthesis and Raman spectroscopic study of Mg/Al, Fe hydrotalcites with variable cationic ratios, *J. Raman Spectrosc.*, 2009, **40**, 1138–1143.

37 V. Rives, *Layered Double Hydroxides: Present and Future*, Nova Publishers, 2001.

38 B. S. Murty, J. W. Yeh, S. Ranganathan and P. P. Bhattacharjee, *High-entropy Alloys*. Elsevier, 2nd edn, 2019.

39 Y. Zhang, *High-Entropy Materials*, Springer Singapore: Singapore, 2019, p. 113.

40 S. N. Golovin, M. N. Yapryntsev and O. E. Lebedeva, Hydrothermal Synthesis of Layered Double Hydroxides Doped with Holmium, Thulium and Lutetium, *Inorganics*, 2022, **10**, 217.

41 O. A. Vorontsova, R. N. Saenko and O. E. Lebedeva, Scandium-containing layered hydroxides, *Russ. J. Inorg. Chem.*, 2007, **52**, 1662–1665.

42 E. S. Seliverstov, A. S. Pisarenko, M. N. Yapryntsev and O. E. Lebedeva, Optimal synthetic route for obtaining Co/In layered double hydroxide, *Ceram. Int.*, 2024, 56019–56024.

43 A. Sarkar, B. Breitung and H. Hahn, High entropy oxides: The role of entropy, enthalpy and synergy, *Scr. Mater.*, 2020, **187**, 43–48.

44 E. Lokcu, C. Toparli and M. Anik, Electrochemical performance of (MgCoNiZn) 1–x Li x O high-entropy oxides in lithium-ion batteries, *ACS Appl. Mater. Interfaces*, 2020, **12**, 23860–23866.

45 H. Putz and K. Brandenburg, *Match!–Phase Analysis Using Powder Diffraction, Crystal Impact*, GbR, Kreuzherrenstr, 2016, vol. 102, *p. 53227*.

46 F. Cavani, F. Trifirò and A. J. C. T. Vaccari, Hydrotalcite-type anionic clays: preparation, properties and applications, *Catal. Today*, 1991, **11**, 173–301.

47 A. Fahami, F. S. Al-Hazmi, A. A. Al-Ghamdi, W. E. Mahmoud and G. W. Beall, Structural characterization of chlorine intercalated Mg-Al layered double hydroxides: a comparative study between mechanochemistry and hydrothermal methods, *J. Alloys Compd.*, 2016, **683**, 100–107.